Regulation of defense strategies and host metabolism to survive neonatal infection

Ziyuan Wu[1,3], Nguyen Tran Nam Tien[2,3], Ole Bæk[1], Jingren Zhong[1], Björn Klabunde[1], Nguyen Thi Hai Yen[2], Nguyen Phuoc Long[2]*, Duc Ninh Nguyen[1]*

[1]Section for Comparative Pediatrics and Nutrition, Department of Veterinary and Animal Sciences, University of Copenhagen, Denmark

[2]Department of Pharmacology and PharmacoGenomics Research Center, Inje University College of Medicine, Busan 47392, Republic of Korea

[3]Co-first author

*Correspondence to: phuoclong@inje.ac.kr (N.P.L), dnn@sund.ku.dk (D.N.N)

Abstract

Upon infection, mammals utilize either disease resistance, which seeks to eliminate pathogens at the cost of potential tissue damage, or disease tolerance, which reduces physiological damage without killing the pathogen. Newborns, constrained by limited energy reserves, predominantly rely on disease tolerance strategies to cope with infection. However, this approach may fail as pathogen levels surpass a critical threshold, prompting a shift to dysregulated immune responses that can lead to excessive inflammation and, consequently, neonatal sepsis, a condition with significant mortality risk. The mechanisms governing the interplay between disease tolerance and resistance in newborns remain poorly understood. Here, we compare infection defense strategies of sepsis survivors and non-survivors in a *Staphylococcus epidermidis*-infected preterm piglet model, mimicking sepsis in preterm infants. Our findings show that compared to non-survivors, sepsis survivors showed elevated disease resistance during early infection, with a stronger disease tolerance in later stages. In contrast, animals succumbing to sepsis showed limited disease resistance after infection and weaker tolerance phenotype with dysregulated immune responses at later time points, including clear signs of respiratory and metabolic acidosis, together with exaggerated inflammation and organ dysfunctions. Hepatic transcriptomics at euthanasia revealed a strong association of tolerance phenotype in survivors with enhanced oxidative phosphorylation, dampened glycolysis and innate and adaptive immune signaling. Plasma metabolomics confirmed our transcriptomic results, highlighting a tolerance phenotype in neonatal infection survivors. This was characterized by rewired metabolic regulations that emphasize mitochondrial activities, including upregulation of the tricarboxylic acid (TCA) cycle and vital interconnected pathways. Our findings suggest potential mechanisms of host metabolism to control a delicate balance of

defense strategies to survive newborn infection. Further, metabolic regulations related to disease tolerance can be exploited to discover novel therapeutics for neonatal infection.

INTRODUCTION

Early-life infection resulting in neonatal sepsis is one of the leading causes of death in newborns, especially those born prematurely (Fleischmann-Struzek et al., 2018; Milton et al., 2022; Shane et al., 2017). (Shane et al., 2017)The majority of clinical complications during neonatal sepsis result not from the bacterial, fungal, or viral pathogen, but the dysregulated immune responses and subsequent tissue damage (Harbeson et al., 2018b). Shortly after birth, the neonatal innate immune system shows a reduced capacity to produce pro-inflammatory cytokines upon stimulation, especially in preterm infants (Levy, 2007). Preterm infants are likewise born with lower levels of maternally transferred IgG and show lower levels of circulating immune cells. Despite this compromised immune system of preterm infants, their immune systems can still trigger excessive reactions, leading to severe sepsis and septic shock (Wynn and Wong, 2017). This indicates that the development of sepsis in preterm infants cannot be attributed to simple immune immaturity, but has to be interpreted as a result of a dysregulated immune response.

In general, three different defense strategies against microbes have been described in mammals (Medzhitov et al., 2012): 1) avoidance, where animals or humans avoid contact with microbially contaminated food/substances through sight, smell, or memory of previous exposures 2) resistance, which entails active immune responses aiming to eradicate the invading microbe and lastly 3) tolerance, where active immune responses are scaled back in an effort not to eliminate but rather contain the microorganisms to minimize immunopathological damage. Resistance and tolerance are two alternative but complementary host defense strategies and can switch during infection. The

understanding of newborn immunity has shifted in the last decades and mounting evidence shows that newborns heavily rely on tolerance strategy, thus decreasing the host's susceptibility to tissue damage from active resistance. However, it is also clear that once a certain threshold of bacterial loads is reached, a resistance response may become predominant. Newborns exhibit a remarkable capacity to endure circulating bacterial loads that are 10 to 100 times greater than adults can withstand, but also are more prone to severe sepsis and septic shock following infections (Harbeson et al., 2018a; Shane et al., 2017; Yagupsky and Nolte, 1990). This highlights a reliance on tolerance and a higher threshold for active resistance in neonates. In part, this neonatal reliance on tolerance is thought to be necessary for initial post-natal survival following exposure to the microbe-filled extrauterine world, but may also be affected by the unique metabolic demands of early life. Neonates are born with low levels of fat, glycogen, and muscle mass, while the energetic demands for growth and development necessitate maximal energy expenditure even at rest (Boo and Harding, 2007; Levy, 2007). To conserve resources, energy-intensive resistance-type responses may be minimized, with a heightened dependence on tolerance in newborns during septic episodes, reflecting a strategic adaptation to their limited energy reserves (Harbeson et al., 2018b).

Initially considered solely an inflammatory process, sepsis is now also recognized to involve extensive metabolic changes within the host. These serve as a fundamental pathogenicity mechanism and a key factor in the mortality associated with sepsis. This paradigm shift underscores the intricate interplay between metabolism and immunology, extending beyond the simplistic view of metabolic processes merely fueling immunological functions. Upon Toll-like receptor (TLR) stimulation, immune effector cells, including granulocytes, M1 macrophages, cytotoxic and helper T-cells, and NK cells, activate resistance responses and shift to aerobic

glycolysis (also named as "Warburg effect"), necessitating a continuous glucose supply to maintain their inflammatory state during the septic episode (Gaber et al., 2017; Loftus and Finlay, 2016). This heightened energy demand for disease resistance compels neonates to divert resources from essential growth and development, thereby increasing their susceptibility to organ failure due to energy deficits (Harbeson et al., 2018b). Conversely, immune regulatory cells involved in the tolerance response, such as Tregs, M2 macrophages, and memory T cells, adapt by increasing the uptake of exogenous fatty acids and sustaining elevated levels of β-oxidation and oxidative phosphorylation (OXPHOS) (Gaber et al., 2017; Loftus and Finlay, 2016). This adaptation is crucial during infection and sepsis, particularly in newborns, whose unique metabolic demands make these metabolic components of the immune response more critical to their survival. Thus, in the context of neonatal sepsis, the metabolic responses of immune cells assume a pivotal role, potentially exerting a greater influence on morbidity and mortality than observed in adults.

We have previously developed a clinically relevant neonatal sepsis model: Newborn preterm piglets, born at 90% gestation, are inoculated with live *S. epidermidis* bacteria, inducing clinical and paraclinical signs of sepsis, similar to infected preterm infants. (Bæk et al., 2023, 2020b, 2020a; Muk et al., 2022). Using this model, we have demonstrated that high parenteral glucose supply enhances hepatic aerobic glycolysis rates, systemic inflammation, and ultimately, mortality rates, underscoring the critical role of energy metabolism in the progression and outcome of sepsis (Bæk et al., 2023; Muk et al., 2022). If given a standard glucose parental regimen, around 50% of infected animals will succumb to sepsis within 24 hours. In the present study, we investigate how the regulation of disease resistance and tolerance mechanisms interplay with host energy metabolism. We identify that individuals surviving sepsis show enhanced resistance responses at the early stage of infection and a stronger tolerance strategy later in the response than those non-

survivors. Furthermore, compared to those who did not survive, the sepsis survivors demonstrated a superior capability to modulate infection-induced aerobic glycolysis and inflammation alongside augmented energy production at the endpoint. Our study provides a significant advancement in understanding the interplay between sepsis pathogenesis and host adaptive responses, particularly disease tolerance, potentially guiding future strategies to improve disease tolerance as a potential target against neonatal sepsis.

RESULTS

Clinical response disparities between infected survivors and non-survivors

Using *S.epidermidis* infected preterm piglets as a model for septic preterm infants, we explored the clinical, cellular, and molecular responses to *S. epidermidis* infection over 15 h post-inoculation (Fig. 1A). After 15 h, 56% of piglets (15/27 infected piglets) developed sepsis, predefined as arterial blood pH of ≤ 7.1 and/or clinical signs of deep lethargy, respiratory arrest or skin bleeding (Muk et al., 2022). This allowed for the division of piglets into three groups: survival (n = 12), non-survival (n = 15), and uninfected (n = 9).

Clinical parameters from blood gas analyses revealed distinct trajectories between survivors and non-survivors. Survivors showed relatively stable status across the first 12 h, followed by a mild drop of pH, oxygen saturation, and base excess, whereas non-survivors displayed a tendency of respiratory acidosis from 12 h (Fig. 1B-E). Interestingly, blood lactate levels showed a mild increase in survivors at the early stages of infection (3-6 h, 1-3 mM, Fig. 1F), suggesting early enhancement of aerobic glycolysis to provide energy for inflammatory response to eliminate circulating bacteria. This was reversed after 12-15 h as non-survivors started to develop metabolic acidosis, characterized by lactate levels > 5 mM in several animals. Likewise, glucose homeostatic

control was disrupted in non-survivors, as many non-survivors showed blood glucose levels > 10 mM (Fig. 1G). Importantly, non-survivors also displayed signs of multiple organ injuries at the endpoint, including elevated levels of blood urea nitrogen (indicating kidney failure) and liver enzyme aspartate aminotransferase, as well as a significant drop of total blood protein and albumin levels, indicating capillary leakage (Fig. 1H-K). These are all classical signs of organ dysfunction in septic infants (Chen et al., 2023; Li et al., 2021). In summary, survivors showed relatively stable status during the infection, whereas infected non-survivors showed clear signs of both respiratory and metabolic acidosis earlier, accompanied by vascular, kidney, and liver dysfunctions at the endpoint.

Early enhanced resistance and later stronger tolerance responses contribute to infection survival

Next, we aimed to quantify the bacterial burden and cytokine levels in blood over the course of infection. In line with the early enhanced lactate production, infected survivors showed lower bacterial burdens (Fig. 2A) and reduced anti-inflammatory response (IL-10, Fig. 2G) at 3 h post-infectious challenge, compared to non-survivors. This further indicates an enhanced early resistance response, actively eliminating bacteria with an increased aerobic glycolysis rate, leading to lactate production despite adequate oxygen supply. Likewise, survivors showed higher levels of major leucocyte subsets (Fig 2B-D). At later time points, survivors showed a decreased production of pro-inflammatory cytokine than non-survivors (IL-6, Fig. 2F), but a similar level of anti-inflammatory cytokines (IL-10, Fig. 2G), seemingly preventing a hyper-inflammatory response (TNF-α/IL-10 and IL-6/IL-10, Fig. 2H-I).

To confirm different strategies throughout the infection stages of sepsis survivors and non-survivors, we further explored the reaction norms between bacterial burdens and blood pH as well as inflammatory status at 3, 6, and 15 hours post-infection via the reaction norm analysis (McCarville and Ayres, 2018; Medzhitov et al., 2012; Schneider and Ayres, 2008) (Fig. 3 & Fig. S1). First, we generated reaction norms using blood pH as our readout for general health, plotted against the pathogen burdens at each time point. A shallow slope indicates stable blood pH (health maintenance) despite a rising pathogen load, revealing a tolerance response. We found that both survivors and non-survivors exhibited similar slopes at 3 hours, together with previously described differences in bacterial burdens (Fig. 2A, left), suggesting enhanced resistance but not altered tolerance phenotype in infected survivors than non-survivors. This is supported by reaction norms of pro-inflammatory cytokines IL-6 and bacterial load with steeper slopes in survivors at 3 hours (Fig. 3B, left), implying augmented inflammation during the process of bacterial clearance. Importantly, at 6 h, infected survivors maintained a shallower slope than non-survivors in the blood pH-bacterial burden plot without distinct differences in cytokine-bacteria burden (Fig. 3A-B, middle & Fig. S1B, middle), indicating a stronger tolerance response in survivors. At the end of the study of 15 h, a clear distinction in blood pH-bacterial burden plot between the two groups was observed (Fig. 3A, right), suggesting survivors exhibited weaker tolerance than at 3 and 6 hours, while non-survivors showed dysregulated immune responses. Moreover, the steeper slopes in the cytokines-bacterial burden plot further indicated that surviving animals adapted to the infection state to maintain vital organ functions rather than using their energy for antimicrobial efforts (Fig. S1A-B, right).

Collectively, we observed a delicate trajectory of different defense strategies in infected survivors, from exhibiting enhanced resistance at the early stage of infection to a stronger tolerance response and host-pathogen cooperation at the later stage of infection.

Suppressed hepatic aerobic glycolysis but elevated mitochondrial activity in infected survivors

Clinical parameters, markers of organ dysfunctions, bacterial burdens, and inflammatory profiles all suggest that enhanced tolerance but not resistance at the later phase of infection is a key driver of sepsis survival. Next, we aimed to investigate how alterations in the host metabolism regulate the induction of a tolerance phenotype to promote infection survival. As the first step, we performed bulk RNA sequencing (RNA-seq) of the liver tissue of survivors, non-survivors, and uninfected controls. Principal component analysis (PCA) revealed distinct gene expression profiles of un-infected animals, infected survivors, and non-survivors (Fig. 4A). To investigate the important pathways differently regulated between survivors and non-survivors, we employed gene set enrichment analysis (GSEA) with KEGG and GO: BP term enrichment analysis. Using the KEGG database, we discovered that survivors exhibited downregulation of glycolysis/gluconeogenesis as well as multiple immune and inflammatory pathways (including HIF-1α, Th1/Th2, Th17, IL-17 signaling, and various innate immune signaling pathways) (Fig. 4B, Table S1). Conversely, survivors demonstrated upregulation of several pathways related to mitochondrial function, such as oxidative phosphorylation, and nicotinate and nicotinamide metabolism. When validating these findings by utilizing the GO: BP database, we also identified a downregulation of the pyruvate metabolic process and an upregulation of mitochondrial respiratory chain complex assembly and mitochondrial ATP synthesis-coupled electron transport in infected survivors (Fig. S2A, Table S1).

We then examined differentially expressed genes (DEGs) across three groups: survival vs. non-survival, survival vs. uninfected, and non-survival vs. uninfected. Our analysis revealed that survivors exhibited 1404 DEGs (653 upregulated and 751 downregulated genes) relative to non-survival piglets. In contrast, when compared to uninfected piglets, survivors showed 4372 DEGs (2249 upregulated and 2123 downregulated), while the non-survivors demonstrated a significant difference with 6921 DEGs (3503 upregulated and 3408 downregulated) (Fig. S2B-D, Table S1). Based on those dysregulated pathways, we selected a set of 26 DEGs between survival and non-survival piglets involved in glycolytic processes, oxidative phosphorylation, and nicotinate and nicotinamide metabolism (Fig. 4C). Two-thirds of genes involved in oxidative phosphorylation (*COX6A2* and *ATP4B*) and all genes involved nicotinate and nicotinamide metabolism (*NMRK1* and *NUDT12*) were up-regulated in survivors vs. non-survivors. Conversely, most of the genes involved in the glycolytic process were downregulated in survivors. Also, when comparing the two infected groups with uninfected animals (Fig. 4C), the profile of 26 genes related to the 3 key metabolic pathways in survivors tended to be similar to that in uninfected animals. Taken together, the hepatic transcriptomic data suggests an association of increased mitochondrial activity and reduced glycolysis with increased disease tolerance and likelihood for survival.

Plasma metabolome confirms metabolic regulations associated with tolerance phenotype

To further explore the metabolic signatures associated with survival, we performed untargeted global metabolic profiling in plasma collected from animals belonging to the same litters (6 survivors, 4 non-survivors, and 3 uninfected piglets). A total of 754 metabolites were annotated in both positive and negative modes. PCA analysis displayed a clear clustering among the three groups based on all metabolites (Fig. 5A). Of 754 metabolites measured, 70 metabolites mapped to various metabolic pathways were observed to be significantly altered between survivors and

non-survivors ($P < 0.05$, VIP score ≥ 1, Table S2). Among the altered metabolites, 52 (74.3%) were up-regulated, and 18 (25.7%) were down-regulated in survivors compared to non-survivors. A pie chart (Fig. 5B) indicates that most altered metabolites belonged to the lipid (28.6%), amino acid (17.1%), and carbohydrate and energy (15.7%) pathways, followed by nucleotide (14.3%), xenobiotics (8.6%), and peptide (5.7%) metabolic pathways.

Feature-based pathway analysis was conducted using the mummichog algorithm, and 23 pathways were significantly enriched (Table S2). These pathways were primarily associated with amino acid metabolism (D-Amino acid metabolism; Alanine, aspartate and glutamate metabolism; lysine metabolism; Histidine metabolism; and Phenylalanine, tyrosine and tryptophan biosynthesis), and carbohydrate metabolism (Pentose phosphate pathway; Pentose and glucuronate interconversions; and Galactose metabolism). Fatty acid metabolism (Linoleic acid metabolism; Biosynthesis of unsaturated fatty acids; and Arachidonic acid metabolism) were also enriched. To validate and refine the findings from our initial feature-based pathway analysis, we executed a subsequent pathway analysis focusing on seventy molecules with differential abundance (MDA). The top six pathways include arginine biosynthesis, primary bile acid biosynthesis, pantothenate and CoA biosynthesis, citrate cycle (TCA cycle), beta-alanine metabolism, and pyruvate metabolism (Fig 5C-D). Importantly, a majority of the identified pathways are interconnected and ultimately lead to the TCA cycle as a downstream metabolic pathway. Glucogenic amino acids arginine and alanine play a pivotal role in metabolism by entering the TCA cycle and transforming into intermediates that facilitate gluconeogenesis (Hayamizu, 2017). Pantothenate is a crucial precursor for the biosynthesis of coenzyme A (CoA), which is essential for the conversion of pyruvate to acetyl-CoA, and also for the transformation of α-ketoglutarate to succinyl-CoA within the TCA cycle (Leonardi et al., 2005).

To explore specific metabolites involved in amino acid metabolism, carbohydrate metabolism and energy production, and fatty acid β-oxidation, box plots were generated to visualize MDA across three groups (Fig. 5E-G). All metabolites related to carbohydrate metabolism and energy production were upregulated in infected survivors (Fig. 5E). Of note, fumaric and malic acids are intermediates in the TCA cycle and play a crucial role in energy production (Martínez-Reyes and Chandel, 2020). Glycerol 3-phosphate can either enter glycolysis and the TCA cycle or contribute to lipid biosynthesis (Possik et al., 2021). The majority of metabolites associated with amino acid metabolism exhibited upregulation, with the exception of lysine (Fig. 5F). Aspartic acid, glutamic acid, and serine are all glucogenic amino acids that provide fuel for the TCA cycle (Hayamizu, 2017). Furthermore, acylcarnitines including Car 14:1, Car 14:2, Car 18:2, deoxycarnitine, propionylcarnitine, and oleoylcarnitine were all found to be upregulated in survivors (Fig. 5G). Acylcarnitines are involved in the transportation of fatty acids into the mitochondria for β-oxidation, which ultimately leads to the production of acetyl-CoA and provide energy for cell activities (Dambrova et al., 2022). Overall, our data suggests that the TCA cycle and a series of interconnected pathways are enhanced in survivors. This further strengthens hepatic transcriptomic findings of a late tolerance phenotype associated with rewired metabolic regulations to reduce glycolysis and prioritize mitochondrial activities as key mechanisms to survive the neonatal infection.

DISCUSSION

Preterm infants, possessing lower energy reserves compared to term infants and adults, exhibit a distinct defense tolerance phenotype during infectious challenges, as energy is allocated primarily to essential growth and development (Harbeson et al., 2018b). This allocation may lead to a skewed

defense tolerance phenotype, where disease tolerance acts as a protective mechanism in the early stages of infection by mitigating exaggerated immune responses and subsequent tissue damage. However, resistance and tolerance are both essential strategies in the battle against infections, each serving distinct roles in the mechanisms against pathogens in animals. By limiting pathogen growth and reproduction, resistance can reduce further transmission of the pathogen and, thus, disease prevalence in the host (Schneider and Ayres, 2008). However, if resistance response is not properly regulated, exaggerated inflammation may occur, leading to severe tissue damage and potentially sepsis. In this study, we proposed that initiating a resistance response through immune-metabolic regulators during early neonatal infection could prevent excessive bacterial proliferation in infected survivors. However, survivors are likely to demonstrate an enhanced tolerance response, characterized by regulated inflammation and minimized tissue damage at later stages of infection. We have established a model of neonatal CONS sepsis in preterm piglets with a consistent mortality rate of 40-50% during 15 h post-infectious challenge (Bæk et al., 2023; Muk et al., 2022). Septic non-survivors suffer from both respiratory and metabolic acidosis and vascular, kidney, and liver dysfunctions. Importantly, in this model, glucose supply and the degree of systemic glycolysis are the main drivers of disease outcomes (Muk et al., 2022). In this present study, we thereby asked why animals with similar genetic backgrounds and identical rearing regimes can display two distinct outcomes, death or survival, upon infection. We postulated that these two groups of animals may possess distinct host metabolism and defense strategies. Here, we discovered that infected survivors were able to exhibit stronger antimicrobial, glycolytic, and immune responses during the first 3 hours of infection to control the prevalence of invading bacteria. This early enhancement of resistance was followed by a stronger tolerance phenotype

during later infection, as demonstrated by similar bacterial burdens but better clinical status and glucose homeostatic control from 6-15 h post-infection in survivors compared to non-survivors.

Recognizing varying defense mechanisms throughout infection stages, from early enhanced resistance to later stronger tolerance in survivors, may have important implications for clinical practice and the development of novel therapeutic strategies. The current study shows that the increased resistance response during the first few hours post-challenge resulted in better clinical outcomes during later stages of infection, as demonstrated by reduced blood acidity and fewer respiratory difficulties in survivors than non-survivors. However, if an anti-inflammatory therapy is initiated in this critical early phase of infection, resistance response may be inhibited, leading to potential bacterial overgrowth later and worsening clinical outcomes. This has been observed in many previous studies in the rodents (Hast et al., 1996; Nedeva et al., 2019; Weng et al., 2011) as well as in our own laboratory when we found that the anti-inflammatory Inter Alpha Inhibitor protein at the early phase of infection exacerbated sepsis outcomes (Bæk et al., 2023). Similar mechanisms may also explain why many randomized controlled trials testing immune suppressive sepsis therapies did not succeed (Angus, 2011; Cohen et al., 2012; Fisher et al., 1996, 1994; Reinhart et al., 2004; Tracey et al., 1987).

Early resistance response observed in infected survivors in this study is associated with increased blood lactate, a marker of increased glycolysis, diminished anti-inflammatory response (IL-10 levels) as well as a high correlation coefficient between bacterial burden and pro-inflammatory cytokines. Immune effector cells, such as macrophages, exert resistance response via a metabolic switch from oxidative phosphorylation to aerobic glycolysis upon TLR stimulation, and require a steady glycolytic flux to maintain the inflammatory phenotype (Gaber et al., 2017). The most immediate consequences of aerobic glycolysis are increased intracellular and extracellular lactate

concentrations (Liberti and Locasale, 2016). However, prolonged resistance phenotype causes significant risks of collateral tissue damage via unspecific immune responses. Therefore, maintenance of disease tolerance at the later phase of infection is crucial for host survival. In this study, from 6h to the end of the study, survivors clearly exhibited better clinical outcomes, less inflammatory response and organ injuries. Evidence of enhanced tolerance in survivors at the euthanasia time point was strongly supported by liver transcriptomics and plasma metabolomics. In our transcriptomic analysis, we found a reduced expression of aerobic glycolysis-associated genes and several immune and inflammatory pathways in sepsis survivors, whereas oxidative phosphorylation and nicotinate and nicotinamide metabolism were upregulated in survivors. These regulations likely inhibit vast ATP production, which is necessary for strong immune responses, and instead support the maintenance of organ functions. Similar observations were shown previously in septic patients, demonstrating transcriptomic profiles with highly up-regulated glycolysis and HIF-1α signaling (Bjerkhaug et al., 2021). When conducting plasma metabolomics, we found aberrant metabolic pathways related to the TCA cycle and mitochondrial activities in sepsis survivors. In a study involving over 1000 adult sepsis patients, metabolomics and proteomics analyses of plasma samples identified significant differences in fatty acid transport and β-oxidation, gluconeogenesis, and the TCA cycle between survivors and nonsurvivors, highlighting potential metabolic targets for improving patient outcomes (Langley et al., 2013). As such, therapeutics, macronutrients, or supplements that support these energy-generating metabolic pathways may be a viable option to reduce morbidity from neonatal sepsis.

Despite significant observations, there are certain limitations that need to be acknowledged. First, it was not possible to characterize host metabolism at several time points during the infection course to obtain a more comprehensive view of metabolic pathways connected to early resistance

response in survivors. Second, acknowledging the advantage of using pigs with a more similar immune system to that in humans (compared to rodents), crossbred preterm piglets do not have an identical genetic background. Therefore, genetic differences may contribute to sepsis survival. Lastly, our preterm sepsis model mimics neonatal CONS infection in preterm infants, and it cannot be excluded that neonatal infection with other bacterial species may exhibit different patterns of defense strategies between survivors and non-survivors. In conclusion, our findings demonstrate potential immune-metabolic mechanisms regulating distinct trajectories of defense strategies to survive neonatal infection. This study emphasizes the importance of the relationship between early resistance response and later tolerance associated with prioritized host metabolism on mitochondrial activities. The study also highlights the potential of using infection therapeutics targeting host metabolism to improve disease tolerance. However, the time for therapy initiation needs to be carefully considered to avoid interference with early resistance response.

MATERIALS AND METHODS

Study approval

All animal studies and experimental procedures were approved by the Danish Animal Experiments Inspectorate under license number 2020-15-0201-00520. These approvals are in accordance with the EU Directive 2010/63, which governs the legislation for the use of animals in research.

S. epidermidis culture preparation

Originating from frozen stock, the *S. epidermidis* bacteria (isolated from a septic infant) were cultured in tryptic soy broth throughout an overnight period. Following this incubation, bacterial density was accurately gauged using spectroscopic techniques. Based on these measurements, a working solution was meticulously formulated by diluting the culture with the precise volume of sterile saline water.

Animal experimental procedures and intervention

We collected a cohort of thirty-six crossbred preterm piglets (Landrace x Large White x Duroc), born by cesarean section at day 106 (90% gestation, term at day 117) from five healthy pregnant sows. After delivery, the newborn piglets were relocated to the intensive care unit, where they were settled in infant incubators preset to a temperature of 37 °C and supplemented with an additional oxygen flow of 1-2 liters per minute. When needed, animals were resuscitated by Doxapram (0.1 ml/kg im.), Flumazenil (0.1 ml/kg im.), tactile stimulation, and positive airway pressure ventilation, applied as necessary until achieving respiratory stability. Furthermore, each piglet was equipped with a vascular catheter, inserted into the dorsal aorta via the transected umbilical cord, facilitating both the administration of parenteral nutrition (PN), bacterial inoculation, and blood sampling.

Approximately two hours postpartum, all animals received PN, and were categorized based on

birth weight and gender, and then randomized to either receive live *Staphylococcus epidermidis* (*S. epidermidis*, 10^9 CFU/kg, n = 27) or a control saline (n = 9) via an interatrial infusion over 3 minutes. Thereafter, the animals were intensively cared for until the 15-h post-infectious challenge. During this period, animals reaching predefined humane endpoint (sepsis criteria, including arterial blood pH of ≤ 7.1 and clinical signs of deep lethargy, discoloration, and tachypnea) were euthanized for tissue collection and counted as an episode of mortality (non-survival). Blood samples were collected at 3, 6, 12, and 15 h post-bacterial challenge via the arterial catheter for blood gas analysis and hematology, as well as plasma storage for cytokine measurements and metabolomic analyses. For the specific purpose of bacterial enumeration within the blood, samples were drawn through puncture of the jugular vein at the 3, 6, and 15-h time points. Serum samples at euthanasia were used for biochemical analysis.

Euthanasia and organ collection

At humane endpoint or 15 h of post-infection, all piglets were deeply anesthetized with a Zoletil mixture (0.1 ml/kg), which included Zoletil 50 (125 mg tiletamine, 125 mg zolazepam), xylazine (6.25 ml xylazine 20 mg/ml), ketamine (1.25 ml ketamine 100 mg/ml), and butorphanol (2.5 ml butorphanol 10 mg/ml), and were subsequently euthanized with an intracardiac injection of barbiturate. The liver and spleen were collected and preserved (frozen and fixed) during necropsy.

Blood gas, hematology, inflammatory markers, and serum biochemistry

Blood samples at 3, 6, 12, and 15 h underwent routine blood gas analysis utilizing the GEM Premier 3000 (Instrumentation Laboratory, USA). Hematological assessments were conducted with the Advia 2120i Hematology System (Siemens). For the quantification of plasma cytokines, TNF-α, IL-6, and IL-10 were analyzed using porcine-specific DuoSet enzyme-linked immunosorbent assays (R&D Systems). Additionally, serum biochemistry evaluations were

executed using the Advia 1800 Chemistry System (Siemens Healthcare Diagnostics, Tarrytown, NY, USA).

Hepatic RNA-Seq transcriptome analysis

Liver RNA from all animals was extracted using the RNeasy mini kit (QIAGEN, US), and subsequently, whole-transcriptome shotgun sequencing was used for gene expression profiling. Library preparation and sequencing were performed by NOVOGENE services (Cambridge, UK). In brief, RNA-Seq libraries were prepared using 1000 ng of RNA and the VAHTS mRNA-Seq V3 Library Prep Kit for Illumina (Vazyme, Nanjing, PRC). The libraries were sequenced on the Illumina NovaSeq 6000 platform, generating 150 bp paired-end reads. Quality and adapter trimming of raw reads were performed using TrimGalore (Babraham Bioinformatics, Cambridge, UK). The resulting clean reads, approximately 26 million per sample, were aligned to the porcine genome (*Sscrofa11.1*) using Tophat2. Gene annotation information for the porcine genome was sourced from *Ensembl* (release 99). The script htseq-count was employed to generate a gene-count matrix.

For differentially expressed gene (DEG) analysis, we excluded weakly-expressed genes and only used protein-coding genes for downstream analysis. The *DESeq2* package version 1.38.3 (Love et al., 2014) was implemented to acquire differentially expressed genes (DEGs) in three comparisons: Survivors *vs.* non-survivors, survivors *vs.* uninfected, and non-survivors *vs*. uninfected. No more covariates were added to the model. Herein, the robust estimation of fold change (FC) using the *lfcShrink* function with *ashr* and false discovery rate (FDR) cut-off of 0.05 were used (Zhu et al., 2019). The volcano plots of total genes were visualized via the *EnhancedVolcano* version 1.14.0 package (Blighe et al., n.d.). The gene set enrichment analysis (GSEA) was used to elucidate the significantly perturbed pathways through the *clusterProfilter* package (version 4.0.2) (Wu et al.,

2021). The FC in expression (log scale) obtained from DEG analysis was used to rank the gene list before introducing them into pathway analyses. Two knowledgebases of the Kyoto Encyclopedia of Genes and Genomes (KEGG) for *Sus scrofa*, and the Biological Processes aspect of Gene Ontology (GO:BP) for *Sus scrofa* were utilized. The FDR cut-off of 0.05 was applied to identify significant pathways. A normalized enrichment score (NES) was obtained in pathway analysis, with either negative or positive values indicating the pathways being down- or up-regulated. The relative expression of pathway-enriched genes was visualized via heatmaps using the *ComplexHeatmap* package version 2.15.1 (Gu et al., 2016). The analysis of liver transcriptomics data was achieved through R 4.2.3 (R Core Team, 2023).

Plasma metabolome analysis

Untargeted metabolomics analysis was performed using ultra-performance liquid chromatography-mass spectrometry (UPLC-MS) via service from Creative Proteomics (Shirley, NY, USA). In brief, the methodology commenced with thawing the samples, followed by transferring 100 µL of each into a 1.5 mL tube and adding 300 µL of pre-cooled methanol. After vortexing the samples for 30 s, they were stored at -20 °C for 1 h and then centrifuged at 9660 *rcf* and 4 °C for 15 min. The supernatant was subsequently transferred to new tubes, stored again at -20 °C for 1 h, and centrifuged under the same conditions. Afterward, 120 µL of the supernatant and 3 µL of DL-o-Chlorophenylalanine (0.5 mg/mL) were prepared in a vial for the instrumental analysis. The analysis was conducted using an ACQUITY UPLC system (Waters, Milford, MA, USA) combined with a Q-Exactive-Plus Hybrid Quadrupole-Orbitrap mass-spectrometer (Thermo, Waltham, MA, USA). Column was ACQUITY UPLC HSS T3 column of 100 mm × 2.1 mm; 1.8 µm (Waters, Milford, MA, USA). Mobile phase A was water with 0.05% formic acid and mobile phase B was acetonitrile. A gradient condition was: 0-1 min, 5% B; 1-12.5 min, 5% to 95% B;

12.5-13.5 min, 95% B; 13.5-13.6 min, 95% to 5% B; 13.6-16 min, 5% B. A fixed flow rate of 0.3 mL/min was used and column temperature was maintained at 40 °C. The sampler was set at 4 °C during the analysis. Mass spectrometry parameters in both positive (POS) and negative (NEG) ion modes included a heater temperature of 300 °C, sheath gas flow rate of 45 arb, auxiliary gas flow rate of 15 arb, sweep gas flow rate of 1 arb, spray voltage of 3.0 kV for POS and 3.2 kV for NEG, capillary temperature of 350 °C, and S-Lens RF levels of 30% for POS and 60% for NEG.

For differential metabolites analysis, only putatively annotated molecules (assigned by the vendor and cross-examination by our team) were used for downstream analyses. To determine molecules with differential abundance (MDA), data first underwent sum normalization and log-transformation without scaling. Subsequently, a litter-adjusted linear model using the *limma* method was leveraged to identify MDAs with the P-value cut-off of 0.05 coupled with the variable of importance (VIP) score of the first component cut-off of 1. Both feature-based functional analysis and MDA-based pathway analysis were leveraged to unveil perturbed pathways. For functional analysis, the mixed ion mode of POS and NEG created by feature-wise merging of retention time, mass-to-charge values, and P-values obtained from statistical analyses of POS and NEG separately were used as input data. MDAs-based pathway analysis with the integration of Fisher's exact test and out-degree centrality was utilized. The knowledgebase from *Sus scrofa* of the Kyoto Encyclopedia of Genes and Genomes (KEGG) was used. Pathways with a P-value cut-off of 0.05 or a gamma-adjusted P-value cut-off of 0.05 and more than one significant hit with respect to functional and pathway analysis were further undergone biological interpretation. All analyses were conducted using *MetaboAnalystR* package version 4.0.0 (Pang et al., 2022) in R version 4.2.3 (R Core Team, 2023).

Statistical analysis

All statistics were executed via R version 4.3.2 (R Core Team, 2023). For discerning differences at specific intervals (3, 6, 12, and 15 h), continuous data underwent analysis via a linear mixed-effects model, incorporating group, gender, and birth weight as fixed factors and litter as a random factor. Another linear mixed-effects model was employed to further probe disparities spanning the entire experimental duration. This model integrated group, time, their interaction, gender, and birth weight as fixed factors, with litter and pig ID as random factors, using *lme4* package version 1.1.35.1 (Bates et al., 2015). Normal distribution, variance homogeneity of residuals, and fitted values were assessed, and if the data did not conform to a normal distribution, logarithmic transformation was applied. If transformation did not achieve normality, the non-parametric Mann-Whitney U test was used instead. To examine different strategies in the infection response of sepsis survivors and non-survivors, reaction norm analysis was performed using blood pH (as a readout for health) and cytokines (as a readout for inflammatory status) at 3, 6, and 15 hours and plotted against the pathogen burdens at the same time point by linear regression. Extra sum-of-squares F Test was used to compare slopes. Statistical significance was defined as P-value < 0.05.

ACKNOWLEDGMENTS

The authors thank Thomas Thymann, Tik Muk, Simone Margaard Offersen, Anders Brunse, Karoline Aasmul-Olsen, Malene Spiegelhauer, Kristina Larsen, Malene Skovsted Cilieborg, Britta Karlsson, and Jane C. Povlsen for the assistance in animal experiments and lab analysis.

The study was funded by Novo Nordisk Foundation (grant number NNF220C0078747). ZY was supported by a PhD grant from the China Scholarship Council.

AUTHOR CONTRIBUTIONS

DNN, OB, ZY, and JR designed the experiments. ZW, JR, OB, and DNN performed the animal experiments. ZY and JR performed laboratory analyses. ZY performed statistical analysis of clinical data, managed raw data, and generated figures and tables. ZY, NT, and HY were responsible for all omics data analysis under DNN and NPL's supervision. ZY, NT, OB, JR, BK, NPL, and DNN were mainly responsible for data interpretation. ZY, NT, OB, NPL, and DNN wrote the first manuscript draft. All authors contributed to data interpretation, manuscript revision, and approval of the final manuscript version.

DECLARATION OF INTERESTS

The authors declare that they have no conflict of interest.

REFERENCES

Angus, D.C., 2011. The Search for Effective Therapy for Sepsis: Back to the Drawing Board? JAMA 306, 2614. https://doi.org/10.1001/jama.2011.1853

Bæk, O., Brunse, A., Nguyen, D.N., Moodley, A., Thymann, T., Sangild, P.T., 2020a. Diet Modulates the High Sensitivity to Systemic Infection in Newborn Preterm Pigs. Front. Immunol. 11, 1019. https://doi.org/10.3389/fimmu.2020.01019

Bæk, O., Muk, T., Wu, Z., Ye, Y., Khakimov, B., Casano, A.M., Gangadharan, B., Bilic, I., Brunse, A., Sangild, P.T., Nguyen, D.N., 2023. Altered hepatic metabolism mediates sepsis preventive effects of reduced glucose supply in infected preterm newborns (preprint). Immunology. https://doi.org/10.1101/2023.09.11.557116

Bæk, O., Ren, S., Brunse, A., Sangild, P.T., Nguyen, D.N., 2020b. Impaired Neonatal Immunity and Infection Resistance Following Fetal Growth Restriction in Preterm Pigs. Front. Immunol. 11, 1808. https://doi.org/10.3389/fimmu.2020.01808

Bates, D., Mächler, M., Bolker, B., Walker, S., 2015. Fitting Linear Mixed-Effects Models Using **lme4**. J Stat Softw 67. https://doi.org/10.18637/jss.v067.i01

Bjerkhaug, A.U., Granslo, H.N., Klingenberg, C., 2021. Metabolic responses in neonatal sepsis—A systematic review of human metabolomic studies. Acta Paediatrica 110, 2316–2325. https://doi.org/10.1111/apa.15874

Blighe, K., Rana, S., Lewis, M., n.d. EnhancedVolcano: Publication-ready volcano plots with enhanced colouring and labeling. R package version, 1(0).

Boo, H.A. de, Harding, J.E., 2007. Protein metabolism in preterm infants with particular reference to intrauterine growth restriction. Archives of Disease in Childhood - Fetal and Neonatal Edition 92, F315–F319. https://doi.org/10.1136/adc.2006.099697

Chen, X., He, H., Wei, H., Chen, F., Hu, Y., 2023. Risk factors for death caused by early onset sepsis in neonates: a retrospective cohort study. Bmc Infect Dis 23, 844. https://doi.org/10.1186/s12879-023-08851-3

Cohen, J., Opal, S., Calandra, T., 2012. Sepsis studies need new direction. The Lancet Infectious Diseases 12, 503–505. https://doi.org/10.1016/S1473-3099(12)70136-6

Dambrova, M., Makrecka-Kuka, M., Kuka, J., Vilskersts, R., Nordberg, D., Attwood, M.M., Smesny, S., Sen, Z.D., Guo, A.C., Oler, E., Tian, S., Zheng, J., Wishart, D.S., Liepinsh, E., Schiöth, H.B., 2022. Acylcarnitines: Nomenclature, Biomarkers, Therapeutic Potential, Drug Targets, and Clinical Trials. Pharmacol Rev 74, 506–551. https://doi.org/10.1124/pharmrev.121.000408

Fisher, C.J., Agosti, J.M., Opal, S.M., Lowry, S.F., Balk, R.A., Sadoff, J.C., Abraham, E., Schein, R.M.H., Benjamin, E., 1996. Treatment of Septic Shock with the Tumor Necrosis Factor Receptor:Fc Fusion Protein. New Engl J Med 334, 1697–1702. https://doi.org/10.1056/NEJM199606273342603

Fisher, C.J., Jr, Dhainaut, J.F., Opal, S.M., Pribble, J.P., Balk, R.A., Slotman, G.J., Iberti, T.J., Rackow, E.C., Shapiro, M.J., Greenman, R.L., et al., 1994. Recombinant human interleukin 1 receptor antagonist in the treatment o f patients with sepsis syndrome. Results from a randomized, double-bli nd, placebo-controlled trial. Phase III rhIL-1ra Sepsis Syndrome Study Group. JAMA 271, 1836–43.

Fleischmann-Struzek, C., Goldfarb, D.M., Schlattmann, P., Schlapbach, L.J., Reinhart, K., Kissoon, N., 2018. The global burden of paediatric and neonatal sepsis: a systematic review. The Lancet Respiratory Medicine 6, 223–230. https://doi.org/10.1016/S2213-2600(18)30063-8

Gaber, T., Strehl, C., Buttgereit, F., 2017. Metabolic regulation of inflammation. Nat Rev Rheumatol 13, 267–279. https://doi.org/10.1038/nrrheum.2017.37

Gu, Z., Eils, R., Schlesner, M., 2016. Complex heatmaps reveal patterns and correlations in multidimensional genomic data. Bioinformatics 32, 2847–2849. https://doi.org/10.1093/bioinformatics/btw313

Harbeson, D., Ben-Othman, R., Amenyogbe, N., Kollmann, T.R., 2018a. Outgrowing the Immaturity Myth: The Cost of Defending From Neonatal Infectious Disease. Front Immunol 9, 1077. https://doi.org/10.3389/fimmu.2018.01077

Harbeson, D., Francis, F., Bao, W., Amenyogbe, N.A., Kollmann, T.R., 2018b. Energy Demands of Early Life Drive a Disease Tolerant Phenotype and Dictate Outcome in Neonatal Bacterial Sepsis. Front Immunol 9, 1918. https://doi.org/10.3389/fimmu.2018.01918

Hast, H.A., Caplan, M.S., Thomson, R.B., 1996. ANTI-INFLAMMATORY AGENTS DO NOT REDUCE MORTALITY IN MICE WHEN ADMINISTERED AFTER THE ONSET OF SEPSIS OR ENDOTOXEMIA. • 273. Pediatr Res 39, 48–48. https://doi.org/10.1203/00006450-199604001-00292

Hayamizu, K., 2017. Amino Acids and Energy Metabolism, in: Sustained Energy for Enhanced Human Functions and Activity. Elsevier, pp. 339–349. https://doi.org/10.1016/B978-0-12-805413-0.00021-1

Langley, R.J., Tsalik, E.L., Velkinburgh, J.C. van, Glickman, S.W., Rice, B.J., Wang, C., Chen, B., Carin, L., Suarez, A., Mohney, R.P., Freeman, D.H., Wang, M., You, J., Wulff, J., Thompson, J.W., Moseley, M.A., Reisinger, S., Edmonds, B.T., Grinnell, B., Nelson, D.R., Dinwiddie, D.L., Miller, N.A., Saunders, C.J., Soden, S.S., Rogers, A.J., Gazourian, L., Fredenburgh, L.E., Massaro, A.F., Baron, R.M., Choi, A.M.K., Corey,

G.R., Ginsburg, G.S., Cairns, C.B., Otero, R.M., Fowler, V.G., Rivers, E.P., Woods, C.W., Kingsmore, S.F., 2013. An Integrated Clinico-Metabolomic Model Improves Prediction of Death in Sepsis. Science Translational Medicine 5, 195ra95-195ra95. https://doi.org/10.1126/scitranslmed.3005893

Leonardi, R., Zhang, Y., Rock, C., Jackowski, S., 2005. Coenzyme A: Back in action. Prog Lipid Res 44, 125–153. https://doi.org/10.1016/j.plipres.2005.04.001

Levy, O., 2007. Innate immunity of the newborn: basic mechanisms and clinical correlates. Nat Rev Immunol 7, 379–390. https://doi.org/10.1038/nri2075

Li, X., Li, T., Wang, J., Dong, G., Zhang, M., Xu, Z., Hu, Y., Xie, B., Yang, J., Wang, Y., 2021. Higher blood urea nitrogen level is independently linked with the presence and severity of neonatal sepsis. Ann Med 53, 2194–2200. https://doi.org/10.1080/07853890.2021.2004317

Liberti, M.V., Locasale, J.W., 2016. The Warburg Effect: How Does it Benefit Cancer Cells? Trends Biochem Sci 41, 211–218. https://doi.org/10.1016/j.tibs.2015.12.001

Loftus, R.M., Finlay, D.K., 2016. Immunometabolism: Cellular Metabolism Turns Immune Regulator. J Biol Chem 291, 1–10. https://doi.org/10.1074/jbc.R115.693903

Love, M.I., Huber, W., Anders, S., 2014. Moderated estimation of fold change and dispersion for RNA-seq data with DESeq2. Genome Biol 15, 550. https://doi.org/10.1186/s13059-014-0550-8

Martínez-Reyes, I., Chandel, N.S., 2020. Mitochondrial TCA cycle metabolites control physiology and disease. Nat Commun 11, 102. https://doi.org/10.1038/s41467-019-13668-3

McCarville, J., Ayres, J., 2018. Disease tolerance: concept and mechanisms. Curr Opin Immunol 50, 88–93. https://doi.org/10.1016/j.coi.2017.12.003

Medzhitov, R., Schneider, D.S., Soares, M.P., 2012. Disease Tolerance as a Defense Strategy. Science 335, 936–941. https://doi.org/10.1126/science.1214935

Milton, R., Gillespie, D., Dyer, C., Taiyari, K., Carvalho, M.J., Thomson, K., Sands, K., Portal, E.A.R., Hood, K., Ferreira, A., Hender, T., Kirby, N., Mathias, J., Nieto, M., Watkins, W.J., Bekele, D., Abayneh, M., Solomon, S., Basu, S., Nandy, R.K., Saha, B., Iregbu, K., Modibbo, F.Z., Uwaezuoke, S., Zahra, R., Shirazi, H., Najeeb, S.U., Mazarati, J.-B., Rucogoza, A., Gaju, L., Mehtar, S., Bulabula, A.N.H., Whitelaw, A.C., Walsh, T.R., Chan, G.J., Odumade, O., Ambachew, R., Yohannes, Z.G., Metaferia, G., Workneh, R., Biteye, T., Mohammed, Y.Z., Teklu, A.M., Nigatu, B., Gezahegn, W., Chakravorty, P.S., Naha, S., Mukherjee, A., Umar, K.M., Akunna, A.V., Nsude, Q., Uke, I., Okenu, M.-J., Akpulu, C., Mmadueke, C., Yakubu, S., Audu, L., Idris, N., Gambo, S., Ibrahim, J., Chinago, E., Yusuf, A., Gwadabe, S., Adeleye, A., Aliyu, M., Muhammad, Amina, Kassim, A., Mukaddas, A.S., Khalid, R.Y., Alkali, F.I., Muhammad, M.Y., Tukur, F.M., Muhammad, S.M., Shittu, A., Bello, M., Sa Ad, F.H., Zulfiqar, S., Muhammad, Adil, Jan, M.H., Paterson, L., 2022. Neonatal sepsis and mortality in low-income and middle-income countries from a facility-based birth cohort: an international multisite prospective observational study. The Lancet Global Health 10, e661–e672. https://doi.org/10.1016/S2214-109X(22)00043-2

Muk, T., Brunse, A., Henriksen, N.L., Aasmul-Olsen, K., Nguyen, D.N., 2022. Glucose supply and glycolysis inhibition shape the clinical fate of Staphylococcus epidermidis–infected preterm newborns. Jci Insight 7, e157234. https://doi.org/10.1172/jci.insight.157234

Nedeva, C., Menassa, J., Puthalakath, H., 2019. Sepsis: Inflammation Is a Necessary Evil. Front Cell Dev Biol 7, 108. https://doi.org/10.3389/fcell.2019.00108

Pang, Z., Zhou, G., Ewald, J., Chang, L., Hacariz, O., Basu, N., Xia, J., 2022. Using MetaboAnalyst 5.0 for LC–HRMS spectra processing, multi-omics integration and covariate adjustment of global metabolomics data. Nat Protoc 17, 1735–1761. https://doi.org/10.1038/s41596-022-00710-w

Possik, E., Al-Mass, A., Peyot, M.-L., Ahmad, R., Al-Mulla, F., Madiraju, S.R.M., Prentki, M., 2021. New Mammalian Glycerol-3-Phosphate Phosphatase: Role in β-Cell, Liver and Adipocyte Metabolism. Front Endocrinol 12, 706607. https://doi.org/10.3389/fendo.2021.706607

R Core Team, 2023. R: A language and environment for statistical computing. R Foundation for Statistical Computing, Vienna, Austria.

Reinhart, K., Glück, T., Ligtenberg, J., Tschaikowsky, K., Bruining, A., Bakker, J., Opal, S., Moldawer, L.L., Axtelle, T., Turner, T., Souza, S., Pribble, J., 2004. CD14 receptor occupancy in severe sepsis: Results of a phase I clinical trial with a recombinant chimeric CD14 monoclonal antibody (IC14)*: Crit Care Med 32, 1100–1108. https://doi.org/10.1097/01.CCM.0000124870.42312.C4

Schneider, D.S., Ayres, J.S., 2008. Two ways to survive infection: what resistance and tolerance can teach us about treating infectious diseases. Nat Rev Immunol 8, 889–895. https://doi.org/10.1038/nri2432

Shane, A.L., Sánchez, P.J., Stoll, B.J., 2017. Neonatal sepsis. The Lancet 390, 1770–1780. https://doi.org/10.1016/S0140-6736(17)31002-4

Tracey, K.J., Fong, Y., Hesse, D.G., Manogue, K.R., Lee, A.T., Kuo, G.C., Lowry, S.F., Cerami, A., 1987. Anti-cachectin/TNF monoclonal antibodies prevent septic shock during lethal bacteraemia. Nature 330, 662–664. https://doi.org/10.1038/330662a0

Weng, T.-C., Chen, C.-C., Toh, H.-S., Tang, H.-J., 2011. Ibuprofen worsens Streptococcus pyogenes soft tissue infections in mice. Journal of Microbiology, Immunology and Infection 44, 418–423. https://doi.org/10.1016/j.jmii.2011.04.012

Wu, T., Hu, E., Xu, S., Chen, M., Guo, P., Dai, Z., Feng, T., Zhou, L., Tang, W., Zhan, L., Fu, X., Liu, S., Bo, X., Yu, G., 2021. clusterProfiler 4.0: A universal enrichment tool for interpreting omics data. The Innovation 2, 100141. https://doi.org/10.1016/j.xinn.2021.100141

Wynn, J.L., Wong, H.R., 2017. Pathophysiology of Neonatal Sepsis, in: Fetal and Neonatal Physiology. Elsevier, pp. 1536-1552.e10. https://doi.org/10.1016/B978-0-323-35214-7.00152-9

Yagupsky, P., Nolte, F.S., 1990. Quantitative aspects of septicemia. CLIN. MICROBIOL. REV. 3.

Zhu, A., Ibrahim, J.G., Love, M.I., 2019. Heavy-tailed prior distributions for sequence count data: removing the noise and preserving large differences. Bioinformatics 35, 2084–2092. https://doi.org/10.1093/bioinformatics/bty895

Figures

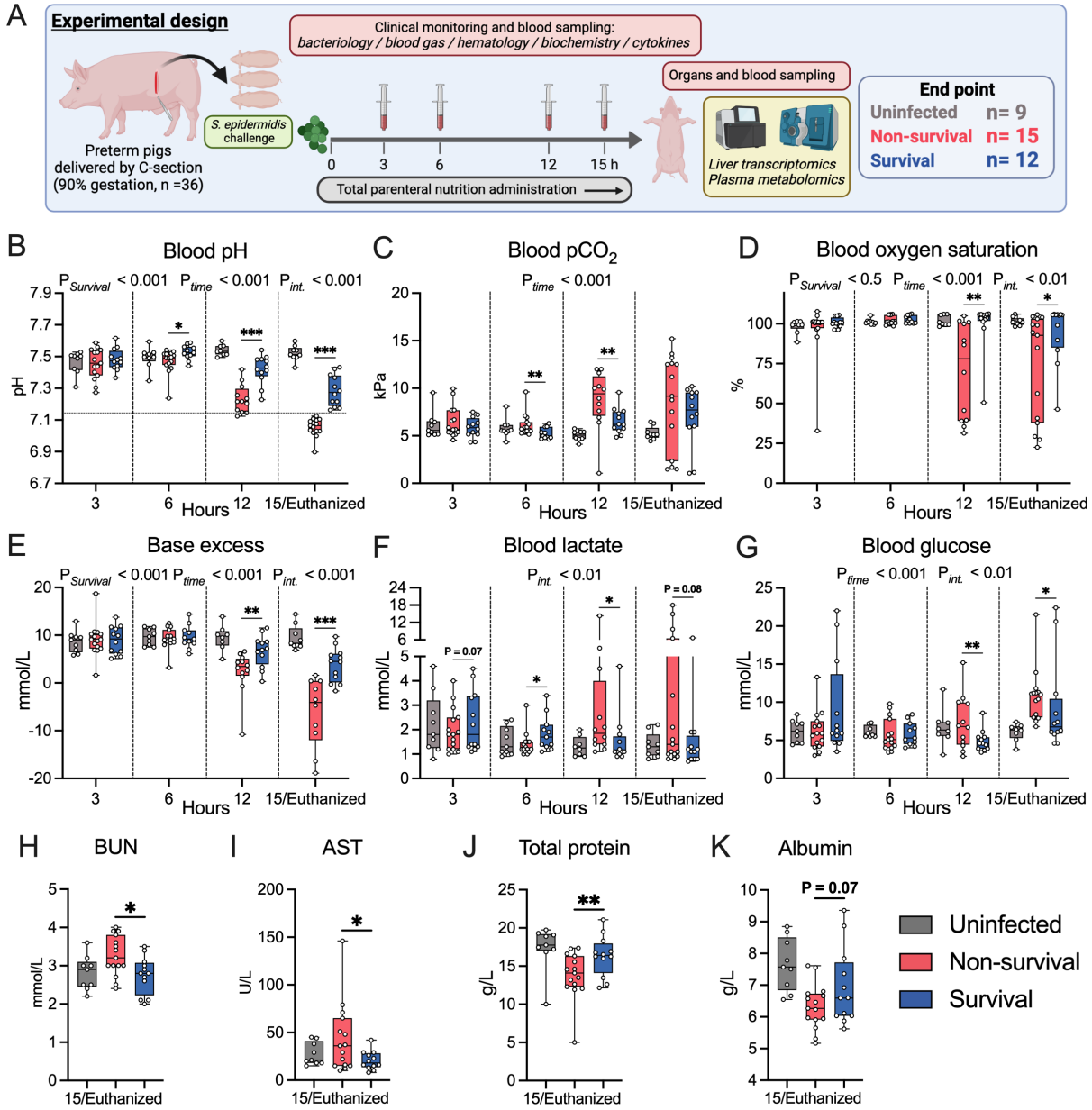
A
Experimental design
Clinical monitoring and blood sampling:
bacteriology / blood gas / hematology / biochemistry / cytokines
Organs and blood sampling
Preterm pigs
delivered by C-section
(90% gestation, n =36)
S. epidermidis
challenge
0
3
6
12
15 h
Total parenteral nutrition administration
Liver transcriptomics
Plasma metabolomics
End point
Uninfected n= 9
Non-survival n= 15
Survival n= 12
B
Blood pH
P Survival < 0.001 P time < 0.001 P int. < 0.001
pH
Hours
C
Blood pCO2
P time < 0.001
kPa
D
Blood oxygen saturation
P Survival < 0.5 P time < 0.001 P int. < 0.01
%
E
Base excess
P Survival < 0.001 P time < 0.001 P int. < 0.001
mmol/L
F
Blood lactate
P int. < 0.01
P = 0.07
P = 0.08
G
Blood glucose
P time < 0.001 P int. < 0.01
H
BUN
I
AST
J
Total protein
K
Albumin
P = 0.07
15/Euthanized
Uninfected
Non-survival
Survival

Figure 1: Clinical response disparities between infected survivors and non-survivors

(A) Schematic of experimental design. Thirty-six cesarean-delivered preterm piglets were randomly assigned to receive either live *S. epidermidis* (10^9 CFU/kg, n=27) or saline (n = 9), were nourished with total parenteral nutrition, and monitored for 15 hours. This setup allowed for the division of piglets into three groups: survival (n = 12), non-survival (n = 15), and uninfected (n = 9) group. Figure created with BioRender.com. **(B-G)** Blood gas parameters (blood pH, blood pCO_2, blood oxygen saturation, blood base excess, blood lactate, blood glucose) collected at 3, 6, 12, and 15 hours post-infection or euthanasia. Dotted horizontal lines specify the principal criterion for humane euthanasia. **(H-K)** Plasma biochemistry parameters (blood urea nitrogen (BUN), aspartate transaminase (AST), total protein and albumin) collected at 15 hours post-infection or euthanasia **(B-K)** Data at each time point were analyzed separately via a linear mixed-effects model, incorporating group, gender, and birth weight as fixed factors and litter as a random factor. *P < 0.05, **P < 0.01, and ***P < 0.001, compared between survival and non-survival groups at the same time point. **(B-G)** Another linear mixed-effects model was employed to further probe disparities spanning the entire experimental duration, incorporating group, time, their interaction, gender, and birth weight as fixed factors, with litter and pig ID as random factors. $P_{Survival}$, P_{time}, and $P_{int.}$ denote probability values for group effect (Survival vs. Non-survival) over time, time effects, and the interaction effects between time and group in the linear mixed effects interaction model, respectively. Statistical significance was defined as P-value < 0.05. All data were presented as box and whiskers plots showing the range from minimum to maximum values.

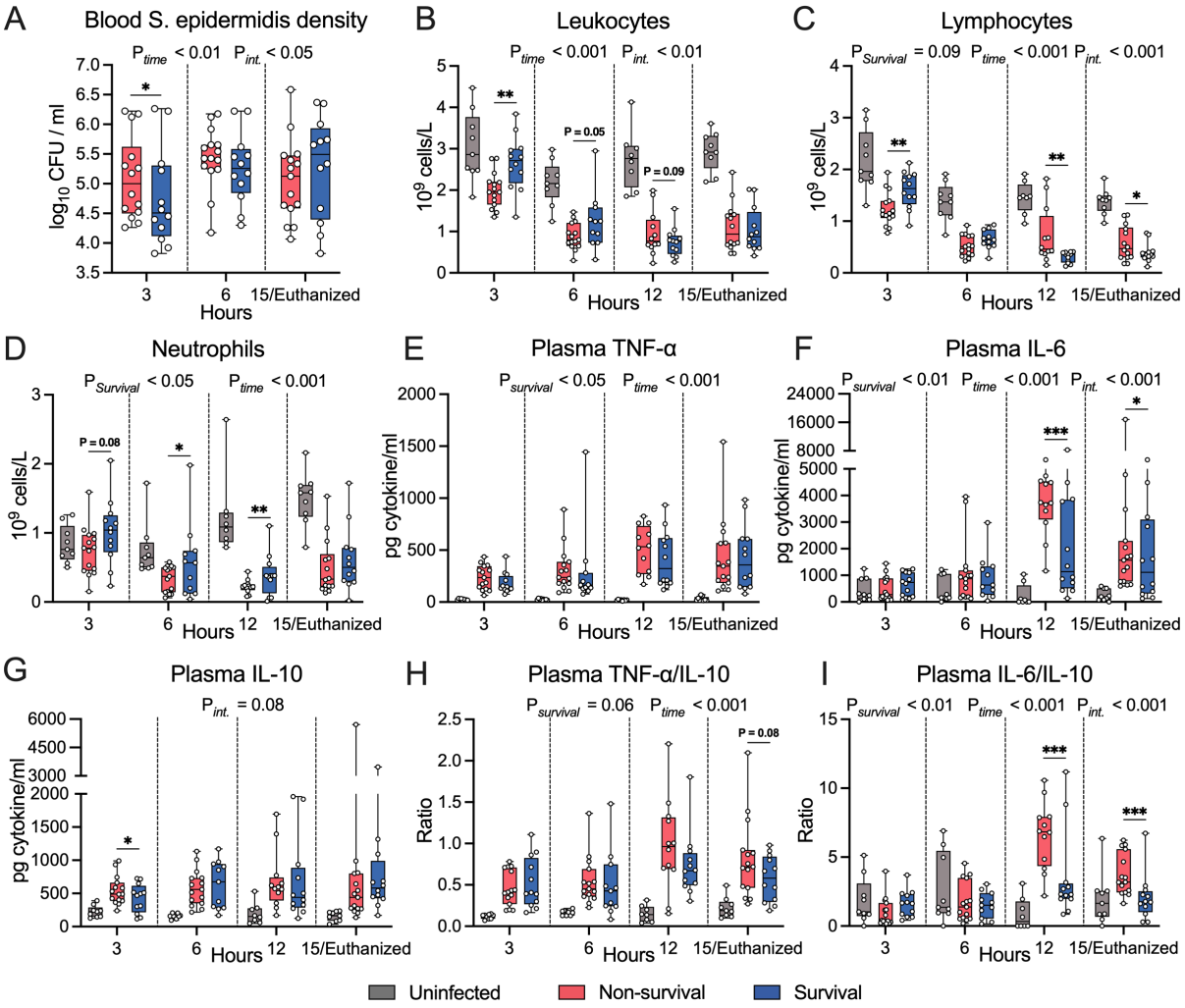
A
Blood S. epidermidis density
P time < 0.01 P int. < 0.05
log10 CFU / ml
Hours
B
Leukocytes
P time < 0.001 P int. < 0.01
10^9 cells/L
P = 0.05
P = 0.09
C
Lymphocytes
P Survival = 0.09 P time < 0.001 P int. < 0.001
D
Neutrophils
P Survival < 0.05 P time < 0.001
P = 0.08
E
Plasma TNF-α
P survival < 0.05 P time < 0.001
pg cytokine/ml
F
Plasma IL-6
P survival < 0.01 P time < 0.001 P int. < 0.001
G
Plasma IL-10
P int. = 0.08
H
Plasma TNF-α/IL-10
P survival = 0.06 P time < 0.001
P = 0.08
Ratio
I
Plasma IL-6/IL-10
P survival < 0.01 P time < 0.001 P int. < 0.001
3
6
12
15/Euthanized
Uninfected
Non-survival
Survival

Figure 2: Bacterial burden, major leucocyte subsets, and cytokine levels in blood over the course of infection

(A) The density of *S. epidermidis* in blood samples, collected via jugular venous puncture at 3 and 6 hours or heart puncture at 15 hours, was determined by counting colony-forming units (CFUs) after plating on tryptic soy agar containing 5% sheep's blood and incubating for 24 hours at 37°C. **(B-E)** Numbers of major leukocyte subsets in blood samples collected 3-15 hours after *S. epidermidis* infusion. **(E-G)** Cytokine levels were measured in heparinized plasma collected at 3, 6, 12, and 15 hours post-infection or euthanasia. **(H-I)** Ratio of TNF-α/IL-10 and IL-6/IL-10, presented as 95% box plots **(A-I)** Data at each time point were analyzed separately via a linear mixed-effects model, incorporating group, gender, and birth weight as fixed factors and litter as a random factor. *$P < 0.05$, **$P < 0.01$, and ***$P < 0.001$, compared between survival and non-survival groups at the same time point. Another linear mixed-effects model was employed to further probe disparities spanning the entire experimental duration, incorporating group, time, their interaction, gender, and birth weight as fixed factors, with litter and pig ID as random factors. $P_{Survival}$, P_{time}, and $P_{int.}$ denote probability values for group effect (Survival vs. Non-survival) over time, time effects, and the interaction effects between time and group in the linear mixed effects interaction model, respectively. Statistical significance was defined as P-value < 0.05. All data were presented as box and whiskers plots showing the range from minimum to maximum values.

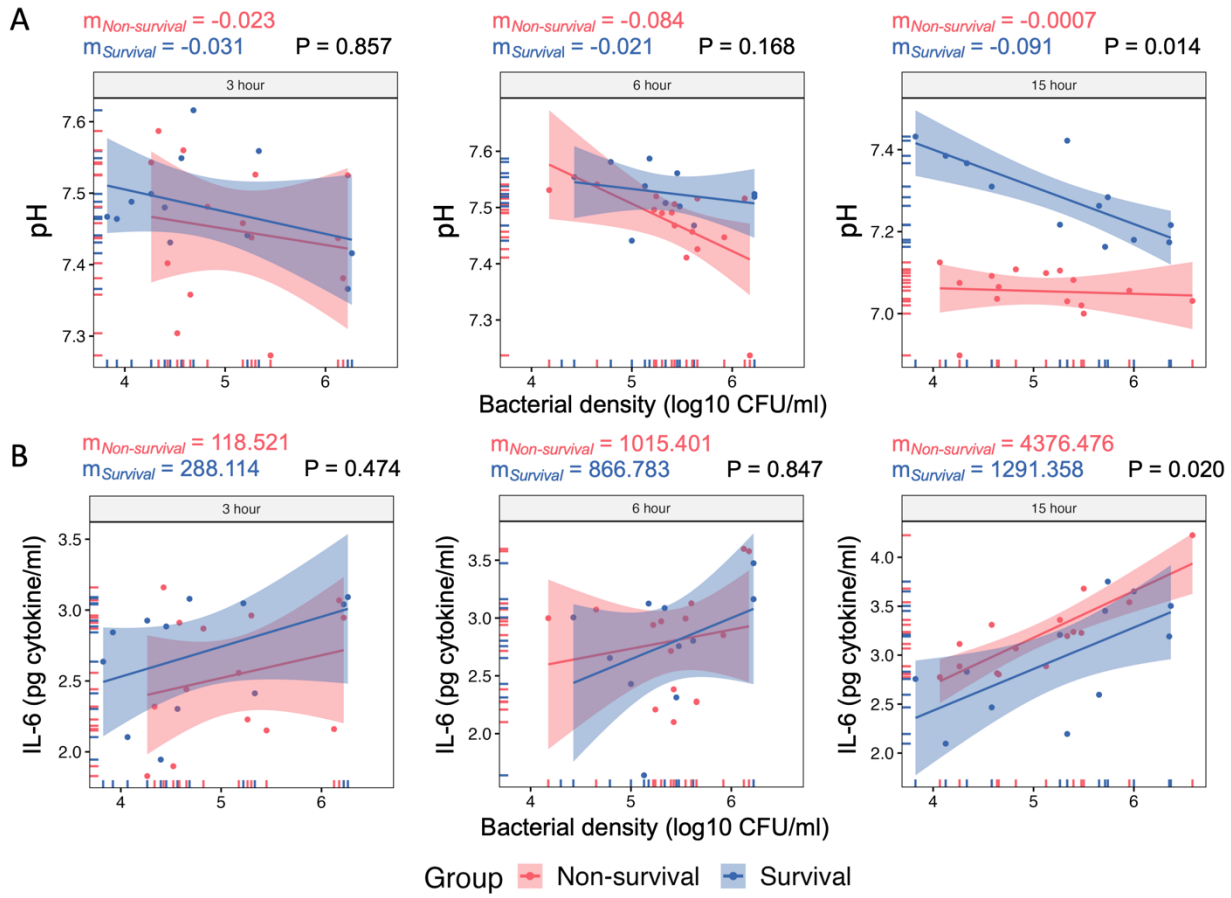

Figure 3: Early enhanced resistance and later stronger tolerance responses contribute to infection survival

(A-B) Reaction norm analysis was performed using blood pH (as a readout for health) and IL-6 (as a readout for inflammatory status) at 3, 6, and 15 hours, and plotted against the pathogen burdens at the same time point by linear regression, respectively. Extra sum-of-squares F Test was used to compare slopes. Statistical significance was defined as P-value < 0.05.

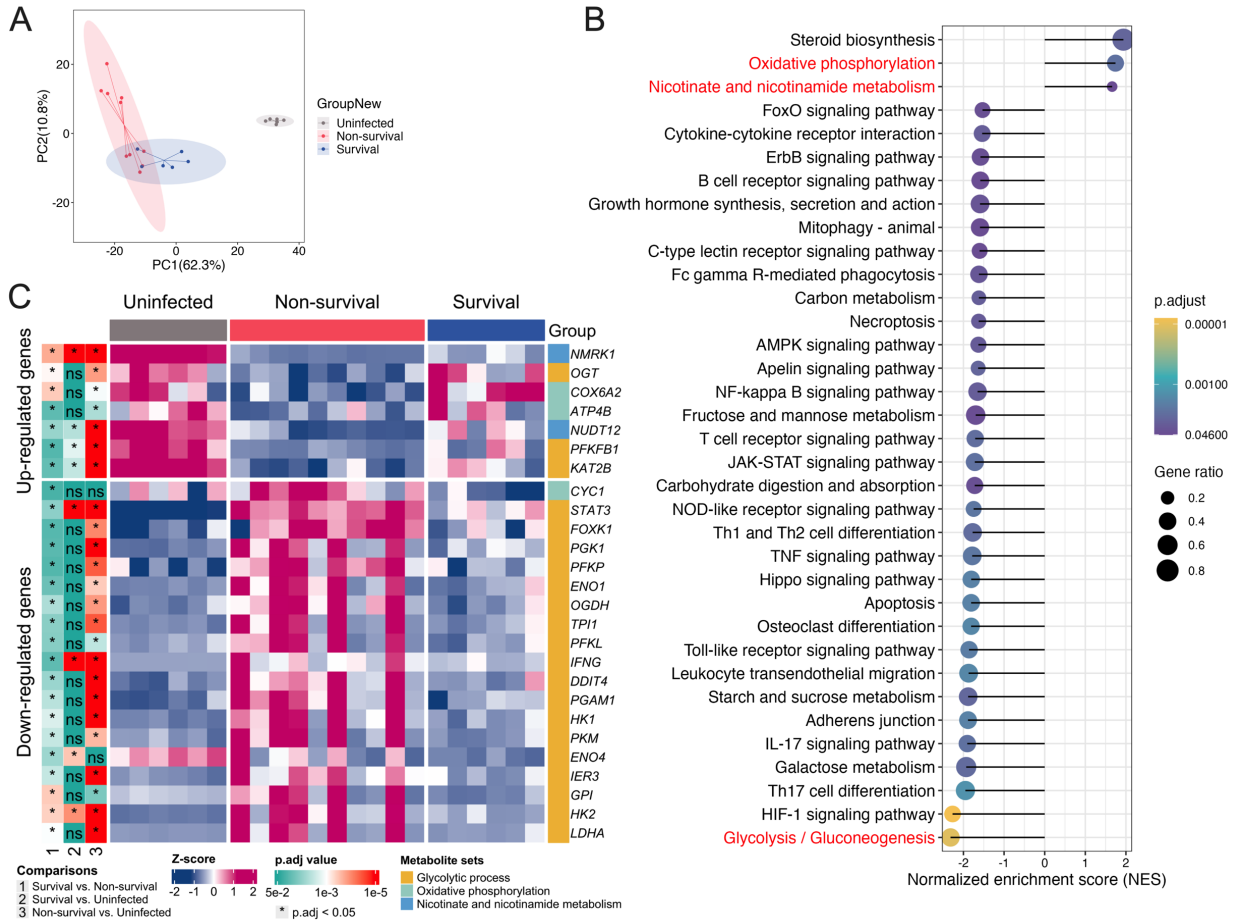

Figure 4: Suppressed hepatic aerobic glycolysis but elevated mitochondrial activity in infected survivors

(A) Principal component analysis (PCA) based on all annotated genes. Scores of the first two principal components from PCA are plotted. **(B)** A gene set enrichment analysis (GSEA) utilizing the KEGG database for *sus scrofa* (pig) was performed to compare survival and non-survival groups, and all-related enriched pathways with significantly expressed categories (adjusted P-value < 0.05 (FDR)) are presented. The size of dots indicates gene ratio while yellow color indicates lower adjusted P-value. **(C)** Heatmaps illustrating 26 DEGs involved in the top enriched pathways between survival and non-survival groups. The label of * represents adjusted P-value < 0.05 (FDR).

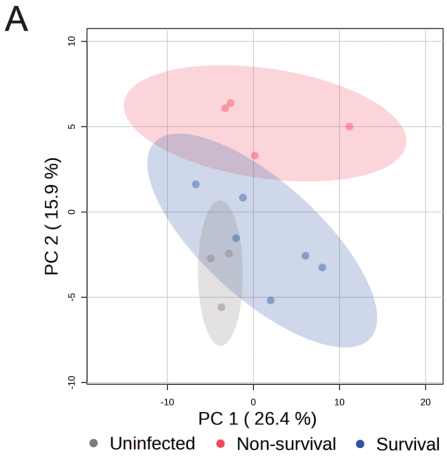

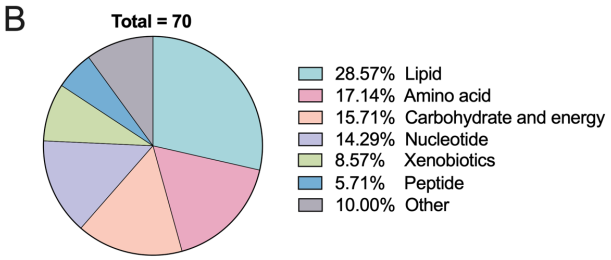

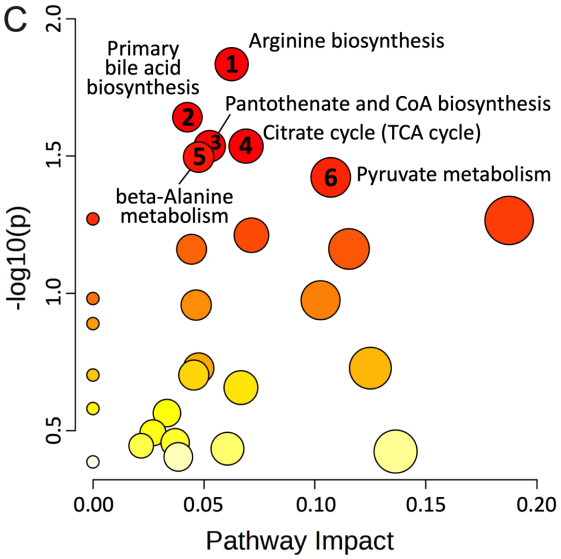

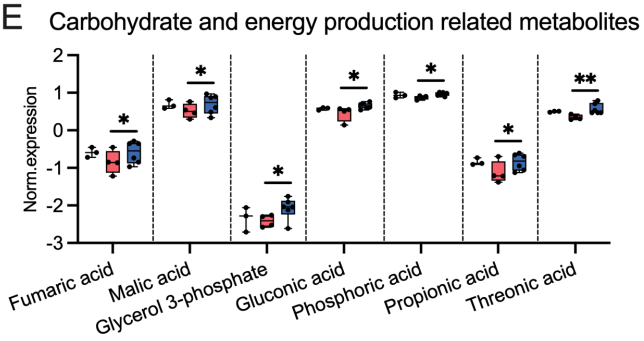

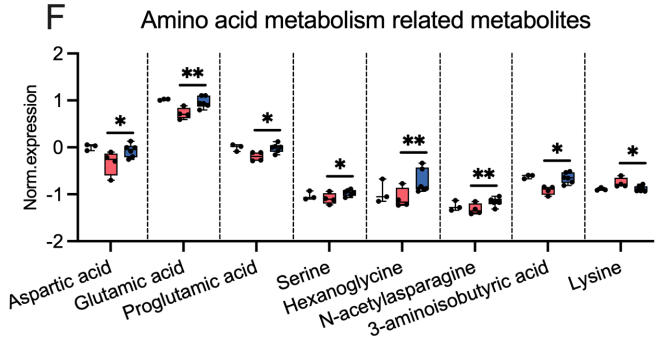

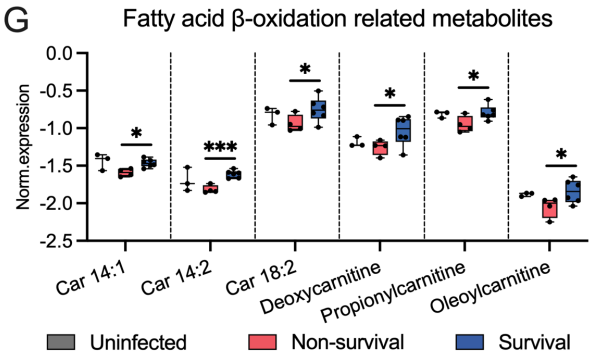

D

No.	KEGG Pathway	Total Comps	Hits	p values	Impact
1	Arginine biosynthesis	14	2	1.46E-02	0.06
2	Primary bile acid biosynthesis	46	3	2.28E-02	0.04
3	Pantothenate and CoA biosynthesis	20	2	2.91E-02	0.05
4	Citrate cycle (TCA cycle)	20	2	2.91E-02	0.07
5	beta-Alanine metabolism	21	2	3.19E-02	0.05
6	Pyruvate metabolism	23	2	3.78E-02	0.11

Figure 5: Plasma metabolome confirms metabolic regulations associated with tolerance phenotype

(A) Principal component analysis (PCA) based on 754 annotated metabolites from both positive and negative modes, with the scores of the first two principal components plotted to illustrate the group separation. **(B)** Pie chart depicting the classification of alerted metabolites between survival and non-survival groups. **(C)** Seventy metabolites with significant differences in abundance between survival and non-survival groups were subjected to the pathway enrichment analysis (y-axis for enrichment P-values, significance of a pathway) and the pathway topology analysis (x-axis for impact values, reflecting centrality and enrichment of a pathway) in the *MetaboAnalystR* package. The color of a circle indicates the level of enrichment significance, with red for high and yellow for low, and the size of a circle is proportional to the pathway's impact value. **(D)** The table presents the top six pathways characterized by P-values with their impacts, highlighting their significance in the study. **(E-G)** Molecules with differential abundance in three main categories were presented as box and whiskers plots showing the range from minimum to maximum values. A litter-adjusted linear model using the *limma* method was leveraged to identify MDAs with the P-value cut-off of 0.05 coupled with the variable of importance (VIP) score of the first component cut-off of 1. *$P < 0.05$ and **$P < 0.01$, compared between survival and non-survival groups at the same time point.